

Deposition of ZnO nanostructured film at room temperature on glass substrates by activated reactive evaporation

D. Yuvaraj · M. Sathyanarayanan ·
K. Narasimha Rao

Received: 9 May 2013 / Accepted: 26 July 2013 / Published online: 20 August 2013
© The Author(s) 2013. This article is published with open access at Springerlink.com

Abstract ZnO nanostructured films were deposited on glass substrates at room temperature by activated reactive evaporation technique. Thermal evaporation of zinc at high deposition rate in presence of oxygen plasma resulted in deposition of ZnO nanostructured film with different flower-like morphologies on glass substrates. The structural and morphological properties of these nanostructured films were studied by XRD, SEM and TEM. A gas phase growth mechanism has been proposed for the formation of nanostructures. The room temperature photoluminescence spectra of these films exhibited weak ultraviolet (UV) and strong broad visible emission peaks. Further, the position of visible emission peak is found to vary with morphology of the grown nanostructured films. Photocurrent measurements indicated that these ZnO nanostructured films show high sensitivity to UV light, and hence can be used as efficient UV photodetectors.

Keywords Activated reactive evaporation · ZnO · Hollow cathode glow discharge tube · Nanoflowers ·

Electronic supplementary material The online version of this article (doi:10.1007/s13204-013-0258-1) contains supplementary material, which is available to authorized users.

D. Yuvaraj (✉) · K. Narasimha Rao
Department of Instrumentation and Applied Physics, Indian
Institute of Science, Bangalore, India
e-mail: yuvaraj@gmail.com

M. Sathyanarayanan
Department of Physics, Anna University, Chennai 600025, India

Present Address:

D. Yuvaraj
Department of Electrical Engineering, London Centre for
Nanotechnology, University College London, London, UK

Nanosheets · Nanoneedles · Photoluminescence · UV
photodetector · Gas phase growth

Introduction

Nanostructured materials possess unique physical and chemical properties and have attracted great research interest in recent years (Edelstein and Cammarata 1996; Xia et al. 2003). Among those materials, zinc oxide, a wide direct band gap semiconductor (3.37 eV) with a large exciton binding energy of 60 meV, high piezoelectric constant and good physical and chemical stability, has been widely studied for potential applications as ultraviolet laser diodes, gas sensors, solar cells and field emission devices (Ozgur et al. 2005; Wang 2004). ZnO crystallizes as wurtzite due to the presence of polar surfaces and preferential growth directions. It has a rich family of unique and peculiar nanostructures (Kong and Wang 2004; Schmidt-Mende and MacManus-Driscoll 2007). Nanostructures with different morphologies such as wires, rods, tubes, belts, plates, flowers and tetrapods have been synthesized by different physical and chemical vapor deposition techniques (Lao et al. 2002; Newton and Warburton 2007; Tang et al. 2006; Umar et al. 2005; Liu et al. 2004; Sun et al. 2004; Kim et al. 2004). Due to larger surface area, sensors and solar cells fabricated using ZnO flower-like nanostructured films exhibited higher sensitivity and efficiency. Jiang et al. (2007) reported that dye sensitized solar cells (DSSc) using photoanodes made of ZnO nanoflowers show higher power conversion efficiency than photoanodes made of ZnO nanorods.

Umar et al. (2005) have grown ZnO nanoflowers on Si substrates maintained at 400–500 °C by thermal evaporation of diethyl zinc (DEZn). Xu et al. (2006) have grown

ZnO nanoflowers on Si substrates by carbothermal reduction of ZnO with graphite at 1,000 °C. Sun et al. (2005) have grown ZnO nanoflowers on Si substrates maintained at 550 °C via oxidation of metallic Zn powder without using metal catalyst. Zhang et al. (2009) have grown rose-like ZnO nanoflowers on SiC substrate at 600 °C by chemical vapor deposition method. All above mentioned evaporation based techniques require high substrate temperatures for growth of nanoflowers and to the best of our knowledge no reports are available on the growth of ZnO nanoflowers at room temperature by evaporation methods.

Among different techniques used for synthesizing nanostructures, gas phase nanostructure synthesis offers a number of advantages compared to conventional growth techniques (Peng et al. 2007; Wang et al. 2008; Shoushtari et al. 2008; Zhang et al. 2006; Dato et al. 2008; Huczko et al. 2002; Balamurugan et al. 2003; Douthwaite 2007). In this technique, nanostructures are synthesized at relatively low temperatures, independent of substrate, and mass production of nanostructures is possible. Currently, ZnO nanorods, nanoneedles, nanowires, carbon nanotubes, graphene and other metal nanoparticles are synthesized using different plasma sources such as microwaves and radio frequencies (Peng et al. 2007; Wang et al. 2008; Shoushtari et al. 2008; Zhang et al. 2006; Dato et al. 2008; Huczko et al. 2002; Balamurugan et al. 2003; Douthwaite 2007). Here, we report activated reactive evaporation (ARE) technique to synthesize flower-like ZnO nanostructures at room temperature. Nanostructures with morphologies such as marigold, rose and sea urchin were grown in the gas phase and deposited as nanostructured film on glass substrate at room temperature. ARE uses a simple experimental setup to synthesize a wide variety of nanostructures by controlling the deposition parameters without using any catalysts, templates or high substrate temperature. Hence, this technique has immense potential to synthesize nanostructured films to make sensors and photo anodes for DSSc (Yuvaraj et al. 2009).

Experimental

The conventional reactive evaporation setup used for ZnO nanostructure synthesis is schematically shown in Fig. 1. Zn was evaporated by resistively heating a tantalum boat containing 2 g of Zn metal beads (Aldrich 99.99 %). A homemade Ebert's type hollow cathode glow discharge (HCGD) source maintained at a potential of 800 V with discharge current of ~100 mA was used to generate oxygen plasma during depositions (Yuvaraj et al. 2009; Lubezky et al. 1987). The rate of Zn evaporation was monitored by a quartz crystal monitor. The glass substrates cleaned using acetone and deionized water in an ultrasonic

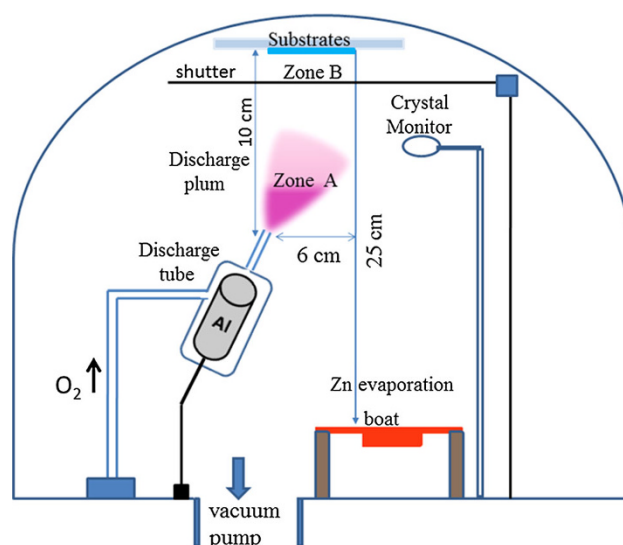


Fig. 1 Schematic illustration of activated reactive evaporation process used for ZnO nanostructured film deposition

bath, and after drying, were loaded onto the substrate holder. Prior to deposition, the chamber having a base pressure of 10^{-3} Pa was maintained at 1×10^{-1} Pa by admitting oxygen gas. Nanostructured films with different morphologies were deposited by varying pressure of oxygen ($2\text{--}5 \times 10^{-1}$ Pa) and evaporation rate of Zn ($40\text{--}60$ Å/s). On achieving optimum deposition conditions [i.e., evaporation rate of Zn ($40\text{--}60$ Å/s)], the shutter near the glass substrate was kept open for 2 min for deposition of nanostructured film.

The structural properties of the nanostructured films were analyzed by X-ray diffraction (XRD, Philips X-ray diffractometer). The morphology and composition of the nanostructured films were observed by field emission scanning electron microscope (FESEM, FEI Sirion) equipped with energy dispersive X-ray analysis (EDAX). The microstructural properties of the nanostructures were evaluated by a transmission electron microscope (TEM, Tecnai F-30). The Raman spectra of these nanostructures were recorded at room temperature (JASCO NRS-1500 W, with an excitation wavelength of 532 nm). Ultraviolet photo-response of these ZnO nanostructured films were studied by measuring photocurrent at room temperature under a constant 5 V DC potential maintained across two well separated aluminum electrodes coated over ZnO films.

Results and discussion

Morphological studies

The morphology observation of the nanostructured films deposited in our experiments showed mainly three

Table 1 Parameters used for deposition of nanostructured films with different morphologies

Film	Deposition conditions	
	Rate of evaporation (\AA s^{-1})	Oxygen partial pressure (mbar)
a	40–44	$2.4\text{--}2.6 \times 10^{-3}$
b	48–50	$2.7\text{--}2.9 \times 10^{-3}$
c	45–48	$4.0\text{--}4.2 \times 10^{-3}$

different morphologies. The parameters used for the deposition of these nanostructured films with different morphologies (films A, B and C) are tabulated in Table 1. Figure 2a (film a) shows several partly and fully-grown marigold-like nanostructures. These flowers are circular in shape and consist of several petal-like structures. The width of the fully-grown flower measured about 1–2 μm in size with height about 1 μm . The inset of Fig. 2a shows the high magnification SEM image of a single marigold-like structure. These flower-like structures contain many ZnO nanosheets (petal-like structures) measuring 100–500 nm in length and 50–100 nm in width and are arranged in an irregular manner with one end attached to the base and other end free to form marigold-like nanostructures. Figure 2b shows the SEM image of rose-like nanostructures deposited on glass substrates (film b). These flowers are arranged randomly and a magnified SEM image of a flower is shown in the inset of Fig. 2b. These flower-shaped structures contain several circular leaves arranged one over the other and the typical diameter of the base plate is about 500–600 nm. The diameter of these circular leaves decreases from base to tip to form flower-like structures. Figure 2c shows the SEM image of sea urchin-like nanostructures grown on glass substrates. These sea urchins measured about 1 μm in size and each sea urchin contains larger number of needle-like nanostructures. These needles measured about ~ 500 nm in length.

Structural studies

XRD studies on the nanostructured films a, b and c revealed that they crystallize as wurtzite ZnO without any other peaks corresponding to impurities or source material Zn. The indexed XRD pattern of the nanostructured films is shown in Fig. 2d. The chemical composition analyzed by EDAX indicated that the as-grown nanostructures contain zinc and oxygen without any catalytic particle (EDAX spectra of ZnO nanostructured film are shown in Fig. 1 in supplementary I). Further, microstructural properties of these films were studied by TEM. Figure 3a, b shows low magnification TEM images of marigold and rose-like nanostructures. We observed that the sample preparation

using sonication did not damage individual flowers. Although TEM is the most powerful and widely used method for performing microstructural studies of nanostructures, it is not ideal for a large sample because of weak penetrability of electrons in large structures. Hence, the growth direction and crystallographic planes of flower-like nanostructures could not be identified to understand the growth of these complex flower-like structures. Figure 3c shows low magnification TEM images of nano sea urchins. From the figure, it is observed that sonication of the sample resulted in breaking of sea urchins into several nanoneedles. HRTEM image of the nanoneedles (Fig. 3d) shows that individual nanoneedles are single crystalline in nature, and further, their growth direction was identified to be along [002].

Raman and photoluminescence studies

The Raman spectra of these nanostructured films a, b and c recorded at room temperature are shown in Fig. 4a. The peaks corresponding to ZnO were observed at ~ 330 , 385, 442 and 585 cm^{-1} . The peak at 330 cm^{-1} was attributed to E_2 high – E_2 low modes and the peak at 385 cm^{-1} is due to the E_2 high mode. The peak at 442 cm^{-1} is attributed to the ZnO non-polar optical high E_2 mode. The peak at 585 cm^{-1} was assigned to the E_1 low mode of ZnO associated with oxygen vacancies in the film. The high intensity of E_1 low (585 cm^{-1}) peak of films a and b deposited at lower oxygen pressure shows large oxygen deficiency when compared to film c deposited at higher oxygen pressure. As the size of the nanostructures is larger by an order higher than the required size for quantum confinement effect, the shift recorded in these films (compared to bulk) may be due to other stress-related effects (Lee et al. 2007).

The PL spectra of ZnO nanostructured films a, b and c with different morphologies recorded at room temperature are shown in Fig. 4b. The PL spectra of these films consist of two emission bands, one in the UV region and other in the visible region. It is well known that UV emission peaks originate from the recombination of free excitons through an exciton–exciton collision process corresponding to near band edge (NBE) emission of wide band gap ZnO (Tang et al. 2006). The impurities and structural defects, such as oxygen and zinc vacancies and interstitials give rise to visible emission peaks (Mei et al. 2004).

For films a and b, which had flower-like morphologies, the UV peak position occurred at 380.6 and 381 nm, and visible peak was centered at 524 and 533 nm, respectively. For film c, the UV and visible emission peaks occurred at 384 and 557 nm, respectively. In all these films, the visible emission peak is dominant than the UV emission peak and the intensity of visible emission was found to be ~ 2 times

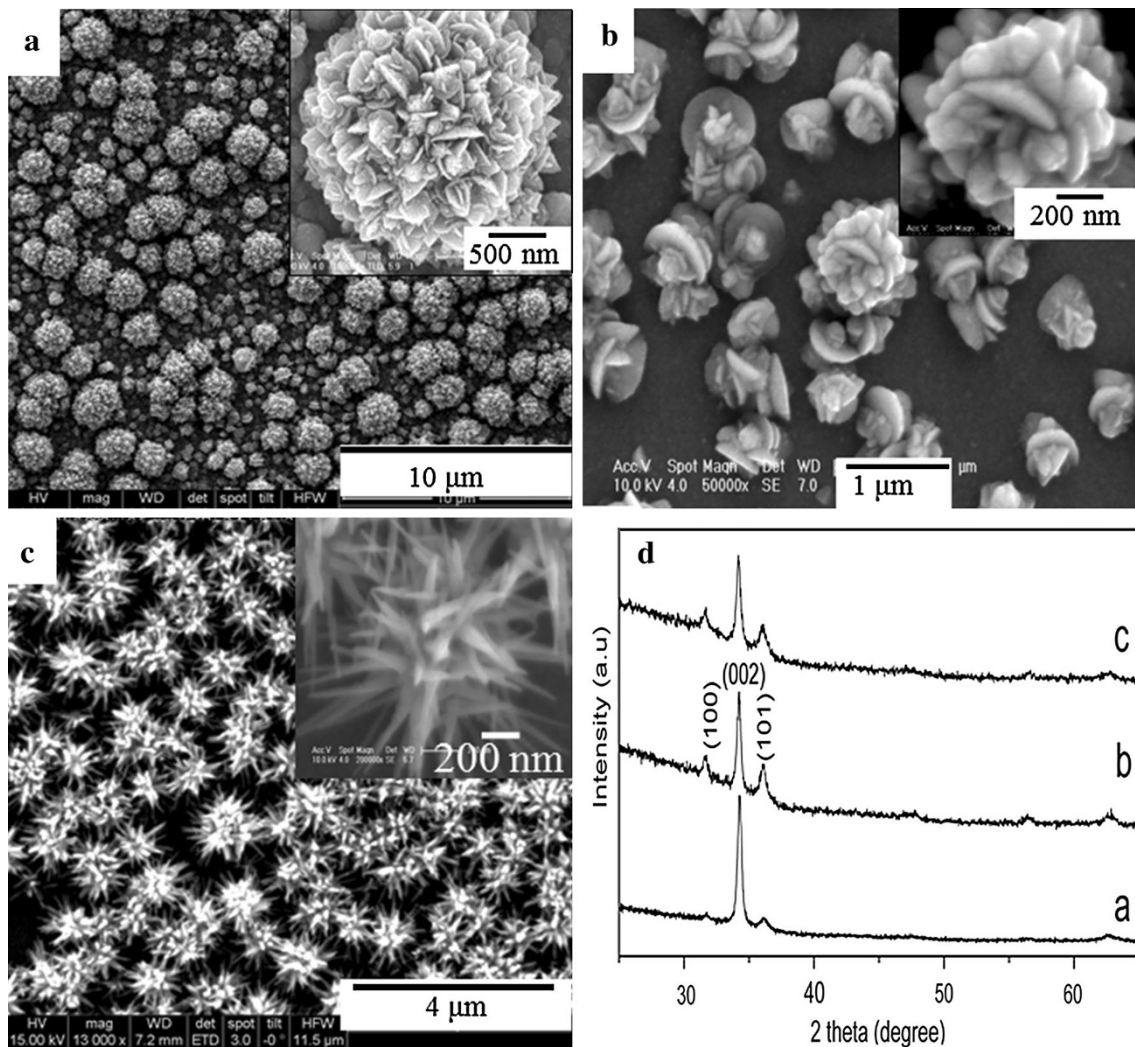


Fig. 2 **a** Low and (*inset*) high magnification SEM image of marigold-like nanostructures (film a). **b** Low and (*inset*) high magnification SEM images of rose-like nanostructures (film b).

c Low and (*inset*) high magnification SEM image of seaurchin-like nanostructures (film c) deposited on glass substrates. **d** Indexed XRD pattern of the ZnO nanostructured films a, b and c

the intensity of UV emission. Hence it is observed that gas phase growth used for growing these morphologies resulted in formation of different structural defects, which in turn gives rise to different visible emission peaks as shown in Fig. 4b.

Growth mechanism

In conventional evaporation process, the ZnO nanostructures are grown at high temperature (400–1,000 °C) on crystalline substrates such as Si, sapphire and quartz, and growth mechanisms such as VLS (Wagner and Ellis 1964) and VS (Sears 1955) have been proposed to explain the growth of these nanostructures. In VLS growth, a suitable catalytic metal particle deposited on the substrates serves as preferential site for growth of nanostructures. Once these catalytic particles were supersaturated with source vapor,

the excess source material precipitates out and grows into 1D nanostructures at the liquid–solid interface. In our growth process, we neither used nor detected any catalytic particle on grown nanostructures, and hence VLS growth is ruled out.

VS mechanism is a catalyst-free process whereby the evaporated vapor condenses and grows into nanostructures either in the gas phase (Gutsch et al. 2005; Height et al. 2006) or on substrates maintained at high temperatures (Peng et al. 2007; Sears 1955). For growing nanostructures by VS mechanism on substrate, high thermal energy (high substrate temperature) is required for the arriving species to diffuse and grow into nanostructures. Usually, the morphology of nanostructures grown by VS mechanism varies with the nature of the substrates. Umar et al. (2005) have reported that ZnO nanoflowers grown by VS mechanism grow with different morphologies on Si (100) and Si (111)

Fig. 3 **a, b** Low magnification TEM image of the marigold and rose-like nanostructures shown in Fig. 2a, b. **c** Low magnification TEM image of the ZnO nano sea urchins and **d** HRTEM image of a ZnO nanoneedle grown along [002]

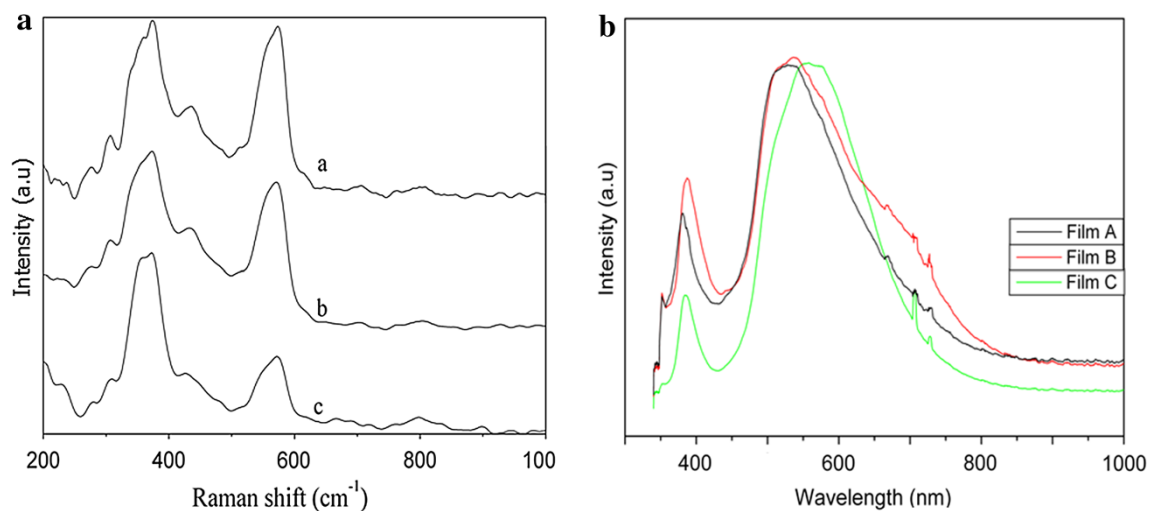
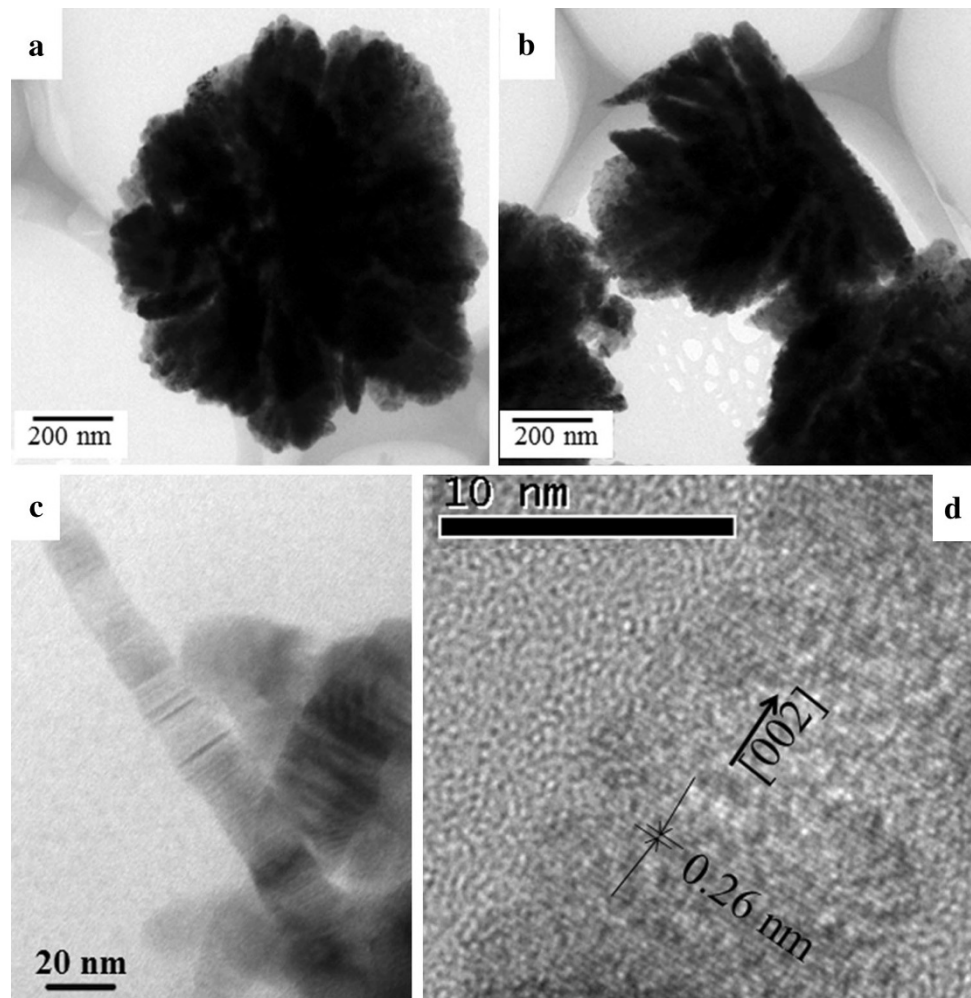


Fig. 4 Raman and PL spectra of ZnO nanostructured films a, b and c deposited on glass substrates recorded at room temperature

substrates under same deposition condition. In our growth process, the nanostructures were grown at room temperature with same morphology irrespective of substrates used

(Yuvaraj et al. 2009). Hence, we propose that the growth of nanostructures takes place in the gas phase during its transit rather than on the substrate (zone A in Fig. 1).

When zinc is evaporated in presence of oxygen plasma, both Zn and oxygen atoms are ionized. These ions react with each other to form ZnO molecules (emission spectra of plasma before and during evaporation of zinc are shown in supplementary II). Under the high density of ZnO molecules, clusters of ZnO were formed in the plasma (zone A) (Gutsch et al. 2005). Nanoflowers are formed as the result of coagulation and anisotropic growth of ZnO clusters in the high density plasma. These nanostructures formed in the gas phase are then transported and deposited as nanostructured film on glass substrates kept above the plasma source (zone B in Fig. 1).

Earlier studies had reported synthesis of nanostructures in gas phase process which had mostly resulted in the formation of 1D nanostructures (Peng et al. 2007; Wang et al. 2008; Shoushtari et al. 2008; Height et al. 2006). In our synthesis, the oxygen flow rate during deposition is relatively very low ($\sim 0.7 \text{ L min}^{-1}$), when compared to other reported gas phase nanostructure syntheses ($\sim 1 \text{ L min}^{-1}$) (Shoushtari et al. 2008; Zhang et al. 2006; Height et al. 2006) (A comparison between the process parameter used in present synthesis and the earlier reports is shown as Table 1 in supplementary-III.). Thus, the mean residence time of the nuclei in plasma is relatively high, resulting in the formation of complex nanoflowers rather than 1D nanostructures as reported by others.

In gas phase nanostructure growth, the morphology of synthesized product depends on pressure, nature of precursor, mean residence time and surface chemistry of the dispersed particle (Gutsch et al. 2005). Recently, Wang et al. (2008) had grown ZnO nanotetrapods, nanowires and nano whiskers in gas phase, by varying the oxygen flow rate (Wang et al. 2008). The change in deposition parameters such as evaporation rate of Zn and pressure of oxygen

causes the variation in Zn/O ratio leading to the formation of different nanostructures as shown in Fig. 2. This gas phase growth method requires further studies to gain more knowledge about the growth and change in morphology as a function of deposition parameters.

Ultraviolet photoresponse of ZnO nanoflowers

UV photoresponse of the ZnO nanostructured films a, b and c deposited on glass substrates was studied at room temperature in ambient atmosphere and vacuum ($5 \times 10^{-3} \text{ Pa}$). Samples used for the photoresponse studies were stored in dark for a week. The linear I - V characteristics of the Al electrode and ZnO nanostructured film show the ohmic nature of the metal–semiconductor contact (inset of Fig. 4 in supplementary IV) (Periasamy and Chakrabarti 2011a, b). Figure 5a shows the time-resolved photocurrent of the ZnO films measured in ambient in response to turn-on and turn-off of the UV light source. The photocurrent of the ZnO nanostructured films increased rapidly when the light was turned on and it become relatively slower with time as shown in Fig. 5a. When the light was turned off after 900 s, the photocurrent decreased at low rate to a lower value. The photocurrent of films a, b and c increased from initial dark value of 0.865, 0.661, and $0.004 \mu\text{A}$ to 9.61, 7.40 and $5.30 \mu\text{A}$, respectively, under UV light illumination for 900 s. The sensitivity of these films is expressed in percentage is defined as $(I_{\text{light}} - I_{\text{dark}})/I_{\text{dark}}$, and is found to be 10, 10 and 1,324 % for films a, b and c, respectively. Figure 5b shows the time-resolved photocurrent of ZnO films measured in vacuum ($5 \times 10^{-3} \text{ Pa}$) in response to turn-on and turn-off of UV light. The increase in photocurrent when UV light was

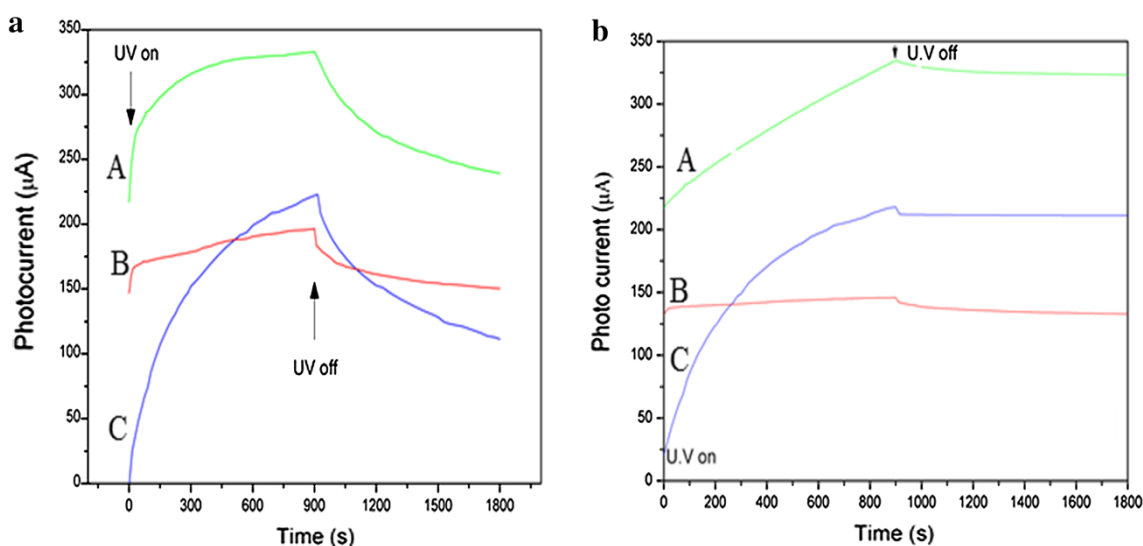


Fig. 5 Time-resolved photocurrent of the ZnO nanostructured films a, b and c measured in ambient and vacuum

turned on follows similar trend to that of ambient atmosphere. When UV light was turned off after 900 s, the photocurrent saturated rather than decreasing for all the films.

The photoresponse of these ZnO nanostructured films under UV light illumination is explained by the following mechanism. In general, the as-prepared ZnO films have n-type conductivity due to the presence of native defects (Jin et al. 2008). These defects serve as shallow donors with a binding energy of 30–60 meV. Oxygen molecules present in ambient atmosphere are adsorbed onto the surface of the ZnO films by capturing a free electron from the n-type ZnO film [O_2 (atmosphere) + e^- (surface) \rightarrow O_2^- (adsorbed)], resulting in decrease of number of charge carriers in the ZnO film. When ZnO film is illuminated with light having energy higher than the band gap of ZnO (3.37 eV), electron–hole pairs are generated. These generated holes combine with negatively charged adsorbed oxygen molecules and releases the oxygen molecules from the surface, resulting in an increase in the free carrier concentration [O_2^- (surface) + h (surface) \rightarrow O_2 (atmosphere)] and hence photocurrent increases during illumination (Fig. 5a). When the light was turned off, both the recombination of the electron–hole and re-adsorption of oxygen molecules from the ambient atmosphere reduce the carrier density, which results in the decrease of photocurrent (Fig. 5a).

The decrease in photocurrent when the UV light was turned off depends on the rate at which oxygen molecules are absorbed onto the surface of ZnO nanostructures. The decrease in photocurrent of these nanostructured films was fitted with first order exponential decay:

$$I(t) = I_d + (I_p - I_d) \exp[-(t/\tau)] \quad (1)$$

where $I(t)$ is the transient current, I_d the current measured in dark, I_p the current measured under UV illumination, t the time after turn-off and τ the corresponding time constant. The time constant (τ) for ZnO nanostructured films a, b and c was found to be 190, 230 and 253 s, respectively. The measured photocurrent in vacuum for the films a, b and c followed similar trend to that ambient when the UV source was turned on, but when the UV source was turned off the photocurrent saturated rather than decreasing. In vacuum (10^{-3} Pa), the number of oxygen molecules is very less (4.83×10^{13} atoms cm^{-3}) compared to the ambient atmosphere (4.83×10^{18} atoms cm^{-3}) and hence the photocurrent saturates due to very slow oxygen re-adsorption process. It is inferred from the photoresponse studies in vacuum that the photo current generation in these nanostructured film is dominated by release and re-adsorption of oxygen molecule on the surface of the ZnO nanostructured films (Jin et al. 2008; Liu et al. 2009; Dhara and Giri 2011).

The change in carrier concentration of ZnO nanostructured film c during UV light illumination was measured by Hall effect measurement setup. Figure 3 in supplementary III shows the plot of carrier concentration measured at different time intervals during turn-on and turn-off of UV lamp. Film c was stored in dark for 2 days before Hall measurement, and the number of charge carriers was found be $3.56 \times 10^{12} \text{ cm}^{-3}$ before UV illumination. The carrier concentration increased with time and was found to be 4.61×10^{-13} and $5.14 \times 10^{14} \text{ cm}^{-3}$ after 5 and 15 min of UV illumination, respectively. When UV light was turned off, the carrier concentration decreased to $1.14 \times 10^{14} \text{ cm}^{-3}$ after 15 min due to re-adsorption of oxygen molecules from the atmosphere (Dhara and Giri 2011). Because of the simplicity in this growth technique and good UV photoresponse, the ARE deposited films have a potential to be used as good UV photodetectors.

Conclusion

ZnO nanoflowers with different morphologies were deposited on glass substrates at room temperature by activated reactive evaporation technique without using metal catalysts or templates. We have proposed a gas phase growth mechanism for the formation of these nanoflowers, wherein the shape and morphology of the nanostructures depend on the evaporation rate of Zn and pressure of oxygen used during deposition. The room temperature photoluminescence spectra of these films exhibited weak ultraviolet (UV) and strong broad visible emission peaks. UV photoresponse studies of these ZnO nanostructured films in ambient atmosphere and vacuum show high sensitivity to UV light.

Open Access This article is distributed under the terms of the Creative Commons Attribution License which permits any use, distribution, and reproduction in any medium, provided the original author(s) and the source are credited.

References

- Balamurugan B, Mehta BR, Shivaprasad SM (2003) “Nanoparticle route” for the synthesis of a stable and stoichiometric Cu_2C_2 phase—a semiconductor material. *Appl Phys Lett* 82:115–117
- Dato A, Radmilovic V, Lee Z, Philips J, Frenklach M (2008) Substrate-free gas-phase synthesis of graphene sheets. *Nano Lett* 8:2012–2016
- Dhara S, Giri PK (2011) Enhanced UV photosensitivity from rapid thermal annealed vertically aligned ZnO nanowires. *Nanoscale Res Lett* 6:504
- Douthwaite RE (2007) Microwave-induced plasma-promoted materials synthesis. *Dalton Trans* 1002–1005
- Edelstein AS, Cammarata RC (1996) *Nanomaterials: synthesis, properties and applications*. Institute of Physics, Philadelphia

- Gutsch A, Muhlenweg H, Kramer M (2005) Tailor-made nanoparticles via gas-phase synthesis. *Small* 1:30–46
- Height MJ, Madler L, Pratsinis SE, Krumeich F (2006) Flame synthesis of ZnO nanorods. *Chem Mater* 18:572–578
- Huczko A, Lange H, Sioda M, Zhu YQ, Hsu WK, Kroto HW, Walton DRM (2002) Hollow cathode plasma synthesis of carbon nanofibre arrays at low temperature. *J Phys Chem B* 106:1534–1536
- Jiang CY, Sun XW, Lo GQ, Kwong DL, Wang JX (2007) Improved dye-sensitized solar cells with a ZnO-nanoflower photoanode. *Appl Phys Lett* 90:263501
- Jin Y, Wang J, Sun B, Blakesley JC, Greenham NC (2008) Solution-processed ultraviolet photodetectors based on colloidal ZnO nanoparticles. *Nano Lett* 8:1649–1653
- Kim HJ, Sung K, An KS, Lee YK, Kim CG, Lee YH, Kim Y (2004) ZnO nanowhiskers on ZnO nanoparticle-deposited Si(111) by MOCVD. *J Mater Chem* 14:3396
- Kong XY, Wang ZL (2004) Polar-surface dominated ZnO nanobelts and the electrostatic energy induced nanohelices, nanosprings, and nanospirals. *Appl Phys Lett* 84:975–977
- Lao JY, Wen JG, Ren YF (2002) Hierarchical ZnO nanostructures. *Nano Lett* 2:1287–1289
- Lee YC, Hu SY, Water W, Huang YS, Yang MD, Shen JL, Tiong KK, Huang CC (2007) Improved optical and structural properties of ZnO thin films by rapid thermal annealing. *Solid State Commun* 143:250–254
- Liu X, Wu X, Cao H, Chang RPH (2004) Growth mechanism and properties of ZnO nanorods synthesized by plasma-enhanced chemical vapor deposition. *J Appl Phys* 95:3141
- Liu CY, Zhang BP, Lu ZW, Binh NT, Wakatsuki K, Segawa Y, Mu R (2009) Fabrication and characterization of ZnO film based UV photodetector. *J Mater Sci Mater Electron* 20:197–201
- Lubezky I, Marcovitch O, Klein Z, Zipin H (1987) Activated reactive evaporation of a transparent conductive coating for the IR region. *Thin Solid Films* 148:83–92
- Mei YF, Fu KY, Siu GG, Chu PK, Li ZM, Yang CL, Ge WK, Tang ZK, Cheung WY, Wong SP (2004) Growth and visible photoluminescence of highly oriented (1 0 0) zinc oxide film synthesized on silicon by plasma immersion ion implantation. *Mat Sci Semicond Process* 7:459–462
- Newton MC, Warburton PA (2007) ZnO tetrapod nanocrystals. *Mater Today* 10:50–54
- Ozgun U, Alivov Ya I, Liu C, Teke A, Reshchikov MA, Dogan S, Avrutin V, Cho SJ, Morkoc H (2005) A comprehensive review of ZnO materials and devices. *J Appl Phys* 98:041301
- Peng H, Fangil Y, Liuyang B, Jinlin L, Yunfa C (2007) Novel rose-like ZnO nanoflowers synthesized by chemical vapor deposition. *J Phys Chem C* 111:194–200
- Periasamy C, Chakrabarti P (2011a) Time-dependent degradation of Pt/ZnO nanoneedle rectifying contact based piezoelectric nanogenerator. *J Appl Phys* 109:054306
- Periasamy C, Chakrabarti P (2011b) Large-area and nano-scale n-ZnO/p-Si heterojunction Photodetectors. *J Vac Sci Tech B* 29(5):1–6
- Schmidt-Mende L, MacManus-Driscoll JL (2007) Nanostructures, defects and devices. *Mater Today* 10:40–48
- Sears GW (1955) A mechanism of whisker growth. *Acta Metallurgica* 3:367–369
- Shoushtari MZ, Parhoodeh S, Farbod M (2008) Fabrication and characterization of zinc oxide nanoparticles by DC arc plasma. *J Phys Conf Ser* 100:052017
- Sun Y, Fuge GM, Ashfold MNR (2004) Growth of aligned ZnO nanorod arrays by catalyst-free pulsed laser deposition methods. *Chem Phys Lett* 396:21
- Sun XH, Lam S, Sham TK, Heigi F, Jurgensen A, Wong NB (2005) Synthesis and synchrotron light-induced luminescence of ZnO nanostructures: nanowires, nanoneedles, nanoflowers, and tubular whiskers. *J Phys Chem B* 109:3120–3125
- Tang ZK, Kawasaki M, Ohtomo A, Koinuma H, Segawa Y (2006) Self-assembled ZnO nano-crystals and exciton lasing at room temperature. *J Cryst Growth* 287:169–179
- Umar A, Lee S, Im YH, Hahn YB (2005) Flower-shaped ZnO nanostructures by cyclic feeding chemical vapor deposition: Structural and optical properties. *Nanotechnology* 16:2462–2468
- Wagner RC, Ellis WC (1964) Vapor-liquid-solid mechanism of single crystal growth. *Appl Phys Lett* 4:89–90
- Wang ZL (2004) Zinc oxide nanostructures: growth, properties and applications. *J Phys Condens Mater* 16:R829–R858
- Wang YG, Sakurai M, Aono M (2008) Mass production of ZnO nanotetrapods by a flowing gas phase reaction method. *Nanotechnology* 19:245610
- Xia Y, Yang P, Sun Y, Wu Y, Mayers B, Gates B, Yin Y, Kim F, Yan H (2003) One-dimensional nanostructures: synthesis, characterization, and applications. *Adv Mater* 15:353–389
- Xu F, Yu K, Li G, Li Q, Zhu Z (2006) Synthesis and field emission of four kinds of ZnO nanostructures: nanosleeve-fishes, radial nanowire arrays, nanocombs and nanoflowers. *Nanotechnology* 17:2855
- Yuvaraj D, Rao KN, Nanda KK (2009) Room temperature synthesis of ZnO nanoneedles by activated reactive evaporation. *J Phys D Appl Phys* 42:035403
- Zhang G, Nakamura A, Nakagawa S, Aoki T, Temmyo J (2006) Growth and characterization of ZnO nanostructures by remote plasma-enhanced metal-organic chemical vapor deposition. *Phys Stat Sol C* 3:722–725
- Zhang N, Yi R, Shi R, Gao G, Chen G, Liu X (2009) Novel rose-like ZnO nanoflowers synthesized by chemical vapor deposition. *Mater Lett* 63:496–499